SCALAR FLUXES FROM URBAN STREET CANYONS. PART II: MODEL

IAN N. HARMAN*, JANET F. BARLOW and STEPHEN E. BELCHER
Department of Meteorology, University of Reading, Earley Gate, P.O. Box 243, Reading, RG6 6BB, U.K.

(Received in final form 19 March 2004)

Abstract. A practical model is developed for the vertical flux of a scalar, such as heat, from an urban street canyon that accounts for variations of the flow and turbulence with canyon geometry. The model gives the magnitude and geometric dependence of the flux from each facet of the urban street canyon, and is shown to agree well with wind-tunnel measurements described in Part I.

The geometric dependence of the flux from an urban street canyon is shown to be determined by two physical processes. Firstly, as the height-to-width ratio of the street canyon increases, so does the roughness length and displacement height of the surface. This increase leads to a reduction in the wind speed in the inertial sublayer above the street canyons. Since the speed of the circulations in the street are proportional to this inertial sublayer wind speed, the flux then reduces with the inertial sublayer wind speed. This process is dominant at low height-to-width ratios. Secondly, the character of the circulations within the street canyon also varies as the height-to-width ratio increases. The flow in the street is partitioned into a recirculation region and a ventilated region. When the street canyon has high height-to-width ratios the recirculation region occupies the whole street canyon and the wind speeds within the street are low. This tendency decreases the flux at high height-to-width ratios. These processes tend to reduce the flux density from the individual facets of the street canyon, when compared to the flux density from a horizontal surface of the same material. But the street canyon has an increased total surface area, which means that the total flux from the street canyon is larger than from a horizontal surface.

The variations in scalar flux from an urban street canyon with geometry is over a factor of two, which means that the physical mechanisms responsible should be incorporated into energy balance models for urban areas.

Keywords: Energy balance, Sensible heat flux, Turbulent transfer, Urban street canyon, Wind tunnel.

1. Introduction

The turbulent vertical fluxes of heat, moisture and momentum play a key role in determining the energy balance of any surface, and therefore in determining the surface temperature and the vertical profiles of the wind and temperature in the boundary layer. The building configuration of urban areas is known to affect the radiative component of the energy balance (Arnfield,

* E-mail: i.n.harman@reading.ac.uk

Boundary-Layer Meteorology **113:** 387–409, 2004.

2003) and the turbulent flux of momentum (Raupach et al., 1991; Grimmond and Oke, 1999b). The sensible heat flux from an urban area depends on the surface type and usage (Grimmond and Oke, 2002). How this dependence relates to differences in the building configuration remains unknown. This knowledge is needed for studies of the near-surface urban air quality and the formulation of the sensible and latent heat fluxes in surface energy balance models of urban areas.

There are a range of existing models for the turbulent fluxes from urban areas, primarily as part of models of the surface energy balance. Grimmond et al. (1991) and Grimmond and Oke (1999a) present an urban surface energy balance model in which the flux of energy into the building fabric and then the turbulent fluxes are related to the evolution of the net radiation. Any influence of the building configuration on the turbulent fluxes is dealt with empirically by training the model with observations to each location. Best (1998, 1999) takes a similar approach by modifying the ground heat flux and allowing the turbulent fluxes to adjust accordingly. What these approaches lack is treatment of how urban geometry affects the physical processes governing the turbulent fluxes.

Many models of the atmospheric processes in an urban area are based on a generic unit of an urban area. One such generic unit is the urban street canyon (Nunez and Oke, 1977). This generic unit is used as the basis of many energy balance models for urban areas (Johnson et al., 1991; Mills, 1993; Sakakibara, 1996; Arnfield and Gimmond, 1998; Masson, 2000; Kusaka et al., 2001; Martilli et al., 2002). Urban street canyon models parameterise the turbulent exchange of heat from the canyon facets to the air above the canyon. The parameterisation is commonly empirical (Kusaka et al., 2001) or based on the turbulent transfer from a horizontal but rough surface (Masson et al., 2002). Most models formulate the fluxes in terms of the wind speed within the street canyon, and a range of methods are employed to parameterise this wind speed. These include invoking results from the studies of flow through vegetation canopies (Masson, 2000), invoking continuity (Mills, 1993), and determining the vertical wind profile through the accumulated effects of drag from a series of street canyons (Martilli et al., 2002). In all cases, the parameterisation of the turbulent flux from the individual facets and the flux from the entire canyon unit needs to be validated.

The flow (Oke, 1988; Baik et al., 2000) and turbulence (Johnson and Hunter, 1995) within an urban street canyon varies with canyon geometry. The turbulent flux of a scalar from the facets of a single urban street canyon is therefore expected to be influenced by canyon geometry. Barlow and Belcher (2002) develop a wind-tunnel method for measuring the facet-averaged flux of a passive scalar in a neutral atmosphere from the street facet of an urban street canyon. Barlow et al. (2004), hereafter referred to as Part I, used this method to measure the facet-averaged flux from each of the facets

of a series of urban street canyons. Narita (2003) measured the flux of a scalar from the facets of a range of canonical geometries using a similar method to Barlow and Belcher (2002). All of these measurements showed a dependence of the fluxes on canyon geometry. The purpose of the present paper is to develop a quantitative model for the turbulent flux of a scalar from an urban street canyon, which can explain the dependence of the fluxes on the geometry of the street canyon that was observed in Part I.

This paper therefore focusses on the geometric dependence of turbulent exchange from an urban street canyon and the physical processes responsible for this dependence. The urban area is represented by a series of street canyons oriented normally to the wind. Consideration is focussed on the case of forced convection. A model for the facet-averaged fluxes from each facet of an urban street canyon in neutral conditions is presented for a range of canyon geometries. The model is developed from ideas on the turbulent transfer across developing boundary layers (Appendix A), and ideas on the geometric dependence of the flow within and above the street canyon (Sections 2 and 3). A comparison between the model predictions and wind-tunnel measurements of Part I then allows an assessment of which physical processes determine the geometric dependence of the turbulent flux of a scalar from an urban surface.

2. Flow Patterns in an Urban Street Canyon

The vertical flux of a scalar, such as sensible heat, from the surface of an urban area in neutral conditions is studied here by considering the flux from a two-dimensional street canyon. A street canyon consists of two parallel, infinitely long, buildings that are uniform in height and have flat roofs. The scalar flux from the urban street canyon is modelled here by considering the facet-averaged flux from each constituent facet. This is done by constructing a network of resistances to the transport of the scalar between the constituent canyon facets and the air in the inertial sublayer (Garratt, 1992). The flow patterns within the urban street canyon are considered now in order to develop the resistance network.

The flow within the urban street canyon can be decomposed into two regions, see Figure 1. Firstly, a *recirculation region* forms in the near wake of each building. Secondly, when the street is sufficiently wide, there is a *ventilated region* downstream of the recirculation region. The different flow characteristics in these two regions mean that the fluxes from these two regions scale differently. In addition, the partitioning of the flow into the two regions depends on geometry, as shown in Figure 1. Hence the model for the turbulent flux of a scalar from an urban street canyon developed here is based on a parameterisation of the flows in these two regions. Figure 2 shows the dimensions of the two regions, together with the nomenclature used.

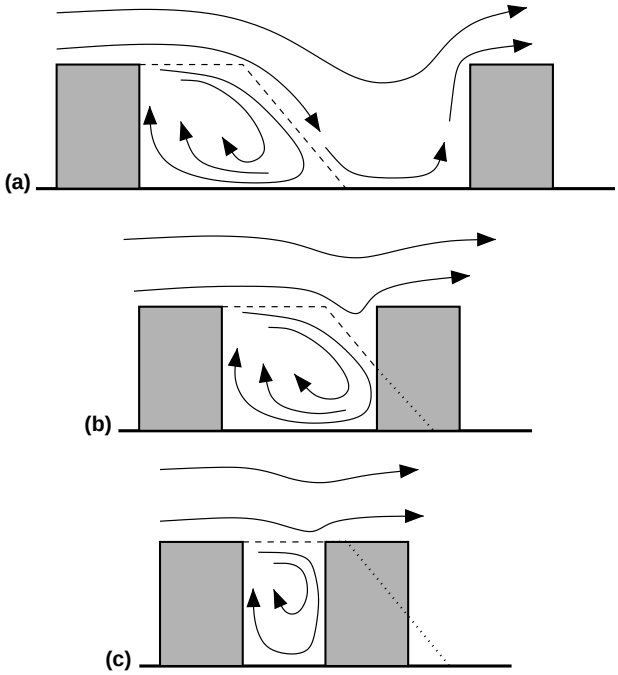

Figure 1. Schematic of the streamlines in the three flow regimes: (a) $L_r < W$ isolated roughness flow regime; (b) $L_r/2 < W < L_r$ wake interference flow regime; (c) $W < L_r/2$ skimming flow regime (flow regimes after Oke (1987)).

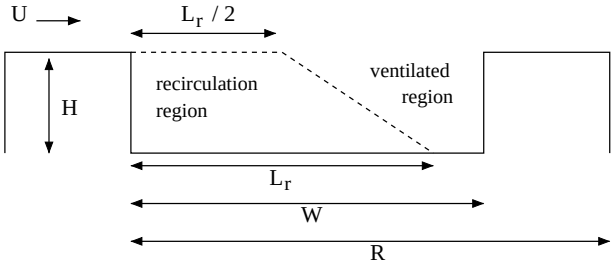

Figure 2. Schematic cross-section of an urban street canyon together with characteristic dimensions of the recirculation region.

The recirculation region is taken here to have a trapezoidal cross-section (Hertel and Berkowicz, 1989). Measurements show that the maximum length of the recirculation region across all canyon geometries, L_r, scales on the height of the building. The value of the ratio L_r/H depends somewhat on the turbulence levels in the boundary layer above and the shape of the buildings and roof. Oke (1987) suggests $L_r/H \approx 2-3$; Castro and Robins (1977) suggest $L_r/H \approx 2$ for cubes; Okamoto et al. (1993) suggest $L_r/H \approx 3.5$ for

the two-dimensional geometry considered here. Here, we therefore take the length of the recirculation region to be $L_r = 3H$.

Oke (1987) describes how three flow regimes arise as the canyon aspect ratio is varied. Figure 1 shows schematically how the division of the street canyon flow varies with geometry and hence how the flow regimes can be related to the length scales of the two flow regions. For wide street canyons, $L_r < W$, so that $H/W < 1/3$, the recirculation region does not impinge on the downstream building (Figure 1a); this is the isolated flow regime of Oke (1987). For intermediate street canyons, $L_r/2 < W < L_r$, so that $1/3 < H/W < 2/3$, and the recirculation region begins to impinge on the downstream building (Figure 1b); this is the wake interference flow regime of Oke (1987). For narrow street canyons, $W < L_r/2$, so that $H/W > 2/3$, and the entire canyon canyon volume is occupied by the recirculation regime (Figure 1c); this is the skimming flow regime of Oke (1987).

Within the ventilated region, when it exists, high speed air from above roof level is brought down to street level. An internal boundary layer then develops along the street surface, and the vertical profile of the wind adjusts to a logarithmic layer in equilibrium with the underlying street surface.

The flow within the recirculation region is driven by the intermittent injection of a high momentum jet associated with the shear layer that is shed off the upstream roof. This jet decelerates as it progresses around the recirculation region due to the entrainment of slower moving air, and due to drag of solid boundaries in a similar way to a rough-boundary wall jet (Townsend, 1976). This picture is supported by observations. Louka et al. (2000) show that the mean vertical velocity at the top of a narrow street canyon is negative in a narrow region next to the downstream wall. The compensating region of positive vertical velocities adjacent to the upstream wall was broader and weaker than the region of negative vertical velocities. A similar pattern of mean vertical velocities at canyon mid-height was found by Caton et al. (2003) in observations of street canyon flow in a water flume. Brown et al. (2000) show that turbulent intensity varies monotonically across a street canyon, with low values adjacent to the upstream wall and high values adjacent to the downstream walls. Finally, Part I (Barlow et al., 2004) showed that the facet-averaged turbulent flux from the downstream wall facet of an urban canyon was, on average, a factor of 2.2 higher than that from the upstream wall facet. All features are consistent with a decelerating wall jet. The strength of the flow within the recirculation region therefore depends on the path length of the jet, which in turn depends on the dimensions of the recirculation region. These arguments explain why wind speeds decrease as the jet circulates from the downstream wall across the street, and then up the upstream wall.

At high canyon aspect ratios, the jet may not reach the street surface. Numerical simulations suggest that weak counter-rotating vortices may then

form in the lowest portion of the street canyon (e.g., Sini et al., 1996; Baik et al., 2000). Hence the wind speeds, and turbulent fluxes, deep in the canyon will be reduced in this flow regime. The effects of these complex processes on the surface fluxes are modelled here by increasing the deceleration of the jet at these high canyon aspect ratios.

3. Resistance Network for an Urban Street Canyon

The previous section described a partitioning of the canyon air flow into recirculating air and ventilated air. This partitioning leads to three pathways for the turbulent transport from the surface to the boundary layer above. These pathways are, firstly, from the wall and street surfaces within the recirculation region to the recirculating air and then aloft; secondly, from the wall and street surfaces within the ventilation region to the ventilated air and then aloft; and, finally, from the roof facet to the air aloft. The ventilated air and recirculating air are each assumed to be independently well mixed and so property X takes a single, but different, value within each of these two air volumes (Nakamura and Oke, 1988). Figure 3 shows the resistance network that we use to represent transport along these three pathways, from the facets of an urban surface to the reference height, z_r, in the inertial sublayer.

Flux balances may now be formed for each of the pathways, as follows. Let F_i denote the flux per unit area of scalar X across the ith resistor in Figure 3.

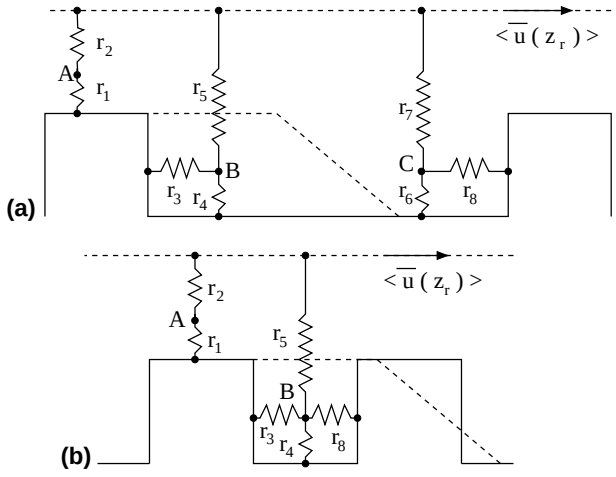

Figure 3. The resistance network for (a) a wide canyon, when there are distinct recirculation and ventilation regions, and (b) a narrow canyon, when there is only a recirculation region. The resistance network for the wake interference regime is the linear interpolation between these two networks.

The flux from the upstream wall and the portion of the street that lies in the recirculation region into the recirculating air (denoted point B in Figure 3) equals the flux out of the recirculation region into the boundary layer aloft, i.e.,

$$HF_3 + \min[L_r, W]F_4 = \min\left[\frac{L_r}{2}, W\right]F_5. \tag{1}$$

Similarly, the flux from the downwind wall and the portion of the street that lies in the ventilated region to the ventilated air (which is denoted point C in Figure 3) equals the flux from the ventilation region to the boundary layer aloft, i.e.,

$$HF_8 + (W - \min[L_r, W])F_6 = \left(W - \min\left[\frac{L_r}{2}, W\right]\right)F_7. \tag{2}$$

The total flux density across the top of the street canyon, F_c, which can be written in terms of a transfer velocity, w_c, i.e. $F_c = w_c \Delta\bar{X}_c$, is then given by,

$$Ww_c \Delta\overline{X}_c = \left(W - \min\left[\frac{L_r}{2}, W\right]\right)F_7 + \min\left[\frac{L_r}{2}, W\right]F_5. \tag{3}$$

Similarly the flux density from the roof, $F_r = w_r \Delta\overline{X}_r$, is given by

$$(R - W)w_r \Delta\overline{X}_r = (R - W)F_2 = (R - W)F_1. \tag{4}$$

Finally the total flux density from the street canyon, $F_t = w_t \Delta\overline{X}_t$, is given by

$$Rw_t \Delta\overline{X}_t = RF_t = (R - W)F_2 + \min\left[\frac{L_r}{2}, W\right]F_5 + \left(W - \min\left[\frac{L_r}{2}, W\right]\right)F_7. \tag{5}$$

The use of the minima of L_r and W or $L_r/2$ and W in Equations (1)–(5) arises as the dimensions of the recirculating region cannot exceed those of the canyon cavity itself. $\Delta\overline{X}$ in Equations (3)–(5) represents the difference between the value X takes at the surface, averaged over the surface area of the individual facets concerned, and the value X takes at the atmospheric reference level, z_r. This formulation shows how the value X takes at one facet can influence the flux from the other facets by changing the value of X at the intermediate points A, B and C.

The fluxes given in Equations (1)–(5) are expressed using the bulk aerodynamic formulation for fluxes (e.g., Garratt, 1992), namely

$$F_X = \Delta\overline{X}/r_X, \tag{6}$$

where r_X is the resistance to transport of property X and $\Delta\overline{X}$ is the difference in the mean values of X across the resistance. The values of the resistances in the network shown in Figure 3 fall into either of two generic types. The resistance to transport from each facet to the intermediate points A, B or C in

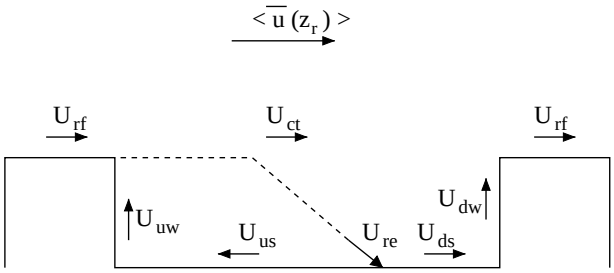

Figure 4. Schematic of the representative winds and their positions.

the figure is determined by that across the internal boundary layer that develops along each facet. The resistance to transport across an internal boundary layer takes the form

$$r_X(z) = \ln\left(\frac{z}{z_{0m}}\right)\ln\left(\frac{z}{z_{0X}}\right)/\langle\bar{u}(z)\rangle, \tag{7}$$

where z is the thickness of the internal boundary layer and $\langle\bar{u}(z)\rangle$ the mean wind speed at distance z away from the surface. The resistance to transport between the intermediate points A, B or C and the reference height z_r is determined by the resistance to transport across a free shear layer. The resistance to transport across a shear layer takes the form

$$r_X(\Delta z) = \Delta\bar{u}/u_*^2, \tag{8}$$

where u_* is a scaling for the local turbulent fluctuations, and is approximated here by that of the overlying inertial sublayer. Equations (7) and (8) are derived fully in Appendix A.

Equations (7) and (8) formulate each of the resistances to transport in terms of the local wind speeds. Therefore all that remains is the specification of wind speeds to parameterise each of the fluxes F_i in Equations (1)–(5). Figure 4 shows the location and nomenclature used for these representative winds. The geometric dependence of the forcing wind speed $\langle\bar{u}(z_r)\rangle$ and these representative wind speeds is considered next.

3.1. Wind profile in the inertial sublayer

The vertical profile of the mean wind in the inertial sublayer of the atmospheric boundary layer, $\langle\bar{u}(z)\rangle$, is characterised by a roughness length and displacement height for the underlying urban surface, namely

$$\langle\bar{u}(z)\rangle = \frac{u_*}{\kappa}\ln\left(\frac{z-d_T}{z_{0T}}\right), \tag{9}$$

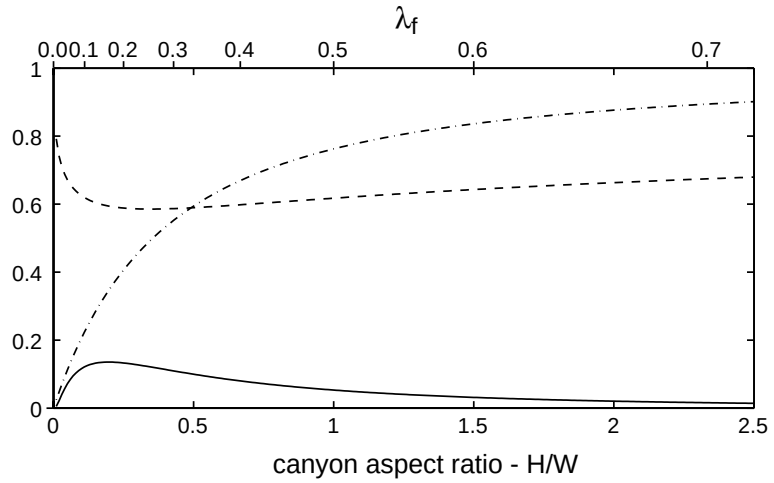

Figure 5. Normalised effective parameters for the vertical profile of the mean wind in the inertial sublayer over a sequence of street canyons calculated from the method of Macdonald et al. (1998). Solid line, roughness length for momentum, z_{0T}/H; dashed-dotted line, displacement height of flow, d_T/H; dashed line, wind speed at twice building height normalised by the free stream flow, $\langle \bar{u}(z_r) \rangle / U_\delta$. The alternative geometric ratio λ_f is the frontal area index (Grimmond and Oke, 1999b) which for square bar geometry is given as $\lambda_f = H/R$.

where κ is the von Kármán constant, taking a value of 0.4, and $u_* = (\tau/\rho)^{1/2}$ is the friction velocity, τ being the turbulent stress. The dependence of the flow in the inertial sublayer on the characteristics of the urban area can be represented by an effective roughness length, z_{0T}, and displacement height, d_T (Grimmond and Oke, 1999a). Macdonald et al. (1998) calculate the vertically integrated drag on an array of cubes and deduce analytical forms for the roughness length and displacement height as functions of the morphological characteristics of the surface. These expressions have many of the observed features of urban roughness lengths and displacement heights (Grimmond and Oke, 1999a). These functions are used here with the morphological characteristics appropriate for two-dimensional street canyons. Figure 5 shows the effective roughness length and displacement height, normalised by the building height, for a series of street canyons with the buildings represented by square bars oriented normally to the wind at varying separations. Figure 5 also shows the wind speed at twice the building height, which we take to be the reference height z_r in the inertial sublayer, normalised by the free-stream wind speed, U_δ, which we take to be the externally imposed forcing to the scalar transport. To facilitate comparison between the model and observations (Section 4) the free-stream wind is taken at the height of the reference wind in the wind tunnel in Part I, i.e., $z_\delta = 9.5H$. Note how, as the canyon aspect ratio increases, there is a rapid decrease and subsequent slow

rise in the wind speed at $z_r = 2H$ due to the combined effects of roughness and displacement.

Cheng and Castro (2002) observe in wind-tunnel studies over an urban-type roughness that when the vertical wind profile is spatially averaged the logarithmic layer observed in the inertial sublayer extends right down to roof level. The wind speed at the reference level, $z_r = 2H$, and wind speed at canyon top, u_{ct}, are then,

$$\langle \bar{u}(z_r) \rangle = \frac{u_*}{\kappa} \ln\left(\frac{2H - d_T}{z_{0T}}\right), \tag{10}$$

$$\frac{u_{ct}}{U_\delta} = \ln\left(\frac{H - d_T}{z_{0T}}\right) \Big/ \ln\left(\frac{z_\delta - d_T}{z_{0T}}\right). \tag{11}$$

We shall see that this variation of wind speed at canyon top with geometry exerts a strong control on scalar transport from the surface.

3.2. Transport from the roof

The resistance to transport from the roof, and indeed each facet, to the intermediate point A represents the resistance to transport across the internal boundary layer that develops along its length. Since the depth of the internal boundary layer grows as the length of the roof facet increases, it follows that the resistances increase with facet length. For simplicity, the depth of the internal boundary layer is taken to be 10% of the facet length.

As for the wind speed at canyon top the representative wind speed for the roof facet, u_{rf}, is obtained by extrapolating the wind profile in the inertial sublayer down to the depth of the internal boundary layer along the roof facet, namely

$$\frac{u_{rf}}{\langle \bar{u}(z_r) \rangle} = \ln\left(\frac{H + \delta_{rf} - d_T}{z_{0T}}\right) \Big/ \ln\left(\frac{z_r - d_T}{z_{0T}}\right). \tag{12}$$

The resistance to transport from the roof facet to this point A in Figure 3, is then given using Equation (7) and the resistance from A to the air aloft using Equation (8), which yields

$$r_1 = \ln\left(\frac{\delta_{rf}}{z_{0m}}\right) \ln\left(\frac{\delta_{rf}}{z_{0X}}\right) \Big/ \kappa^2 u_{rf}, \tag{13}$$

$$r_2 = \frac{\langle \bar{u}(z_r) \rangle - u_{rf}}{u_*^2}, \tag{14}$$

where z_{0m} and z_{0X} are the roughness lengths for momentum and X respectively for the surface material of the roof facet, and u_* is calculated from the wind profile in the inertial sublayer. Finally, δ_{rf} is the thickness of the

internal boundary layer developed along the roof facet, taken as $\delta_{\mathrm{rf}} = \min[0.1(R - W), z_{\mathrm{r}} - H]$.

3.3. Transport from the recirculation region

The measurements of Part I and the fluid dynamical ideas developed in Section 2 motivate a description of the flow in the recirculation region as that of a jet that decelerates as it travels round the canyon. Balancing advection, $u\,\partial u/\partial x$, and turbulent drag, $\tau \sim c_{\mathrm{D}} u^2$ in the jet, yields a flow speed in the jet that decelerates exponentially with distance. There are a number of more sophisticated theoretical descriptions of the deceleration and entrainment of a jet on a flat wall, e.g., Townsend (1976) or Hogg et al. (1997). However, the jet within the street canyon turns corners as it circulates within the canyon and so this work is not immediately applicable. Additionally, these more detailed models add further parameters to the formulation of the flow with no method of determining their value or their geometric dependence. We therefore opt here for the simple exponential description.

First, consider the wind speed of the jet when it first impinges on the street facet, u_{re}. This wind speed is then that at canyon top, u_{ct}, scaled down exponentially to account for entrainment, i.e.,

$$u_{\mathrm{re}} = u_{\mathrm{ct}} \exp\{-\alpha_1 L_{\mathrm{se}}/H\}, \tag{15}$$

where L_{se} is the length of the sloping edge of the recirculation region. The strongest flow along the canyon facets is then located at the end of the recirculation region as observed by Okamoto et al. (1993).

The jet then circulates along the street and wall facets in the recirculation region, and the wind speed varies as

$$u(x) = u_{\mathrm{re}} \exp\{-\alpha_2 x/H\}, \tag{16}$$

where x is the total distance travelled by the jet from the end of the recirculation region. The two exponents α_1 and α_2 are different due to the different physical processes that they represent.

The wind speeds representative of the turbulent flux from the upstream wall, u_{uw}, from the fraction of the street facet in the recirculation region, u_{us}, and from the downstream wall if it is in the recirculation region, u_{dw}, are taken as the average of the flow $u(x)$ along each facet, namely

$$u_{\dagger} = \frac{u_{\mathrm{re}}}{b} \int_a^{a+b} \exp\{-\alpha_2 x/H\}\, dx, \tag{17}$$

where $\dagger$ is one of uw, us or dw, the total distance travelled by the jet to the start of the facet in question is a, and b is the length of the facet. For instance, when considering the transfer from the upstream wall, in the isolated roughness regime $a = L_{\mathrm{r}}$ and $b = H$, in the skimming flow regime $a = W + H$ and $b = H$.

Internal boundary layers of a fixed depth of $0.1H$ are then taken on each facet. The resistances to transport, r_3, r_4, r_5 and r_8 (in the skimming flow regime) are then calculated from Equations (7) and (8) as

$$r_3 = \ln\left(\frac{0.1H}{z_{0m}}\right)\ln\left(\frac{0.1H}{z_{0X}}\right)/\kappa^2 u_{\mathrm{uw}}, \tag{18}$$

$$r_4 = \ln\left(\frac{0.1H}{z_{0m}}\right)\ln\left(\frac{0.1H}{z_{0X}}\right)/\kappa^2 u_{\mathrm{us}}, \tag{19}$$

$$r_5 = \frac{\langle \bar{u}(z_{\mathrm{r}})\rangle - u_{\mathrm{us}}}{u_*^2}, \tag{20}$$

$$r_8 = \ln\left(\frac{0.1H}{z_{0m}}\right)\ln\left(\frac{0.1H}{z_{0X}}\right)/\kappa^2 u_{\mathrm{dw}}, \tag{21}$$

where u_* is the friction velocity calculated from the wind profile in the inertial sublayer. u_{us} is used in Equation (20) and not u_{uw} or u_{dw}, since these are representative wind speeds for the turbulent transfer in the narrow regions next to each wall, whereas r_5 represents the transfer across the top of the recirculation region.

3.4. Transport from the ventilated region

Part of the jet that impinges on the street facet moves along the street facet into the ventilated region. Within the ventilated region high momentum air is mixed downwards so that the jet is only decelerated somewhat. This mechanism is not available in the recirculation region, which therefore has lower wind speeds. The wind speeds representative of the turbulent transport from the downstream fraction of the street, u_{ds}, and the downstream wall in the isolated roughness regime case, u_{dw}, are given as

$$u_{\mathrm{ds}} = \left(\frac{u_{\mathrm{re}}}{W - L_{\mathrm{r}}}\right)\int_0^{W-L_{\mathrm{r}}} \exp\{-\alpha_2 x/H\}\,dx, \tag{22}$$

$$u_{\mathrm{dw}} = \left(\frac{u_{\mathrm{re}}}{H}\right)\int_{W-L_{\mathrm{r}}}^{W-L_{\mathrm{r}}+H} \exp\{-\alpha_2 x/H\}\,dx. \tag{23}$$

As before these wind speeds are taken to be located $0.1H$ away from the facets.

As explained above, the mixing of high momentum air downwards in the ventilated region prevents the turbulent transport in the ventilated region from decreasing to the extent that occurs in the recirculating region. Here this process is represented by placing a minimum bound on the winds speeds calculated using Equations (22) and (23). These bounds are taken from the

wind profile established in an undisplaced boundary layer in equilibrium with the surface when forced by the wind speed u_{ct} at a height $z = H$. The minimum wind speed for u_{ds} is the value taken from this profile at $z = 0.1H$, namely

$$\min u_{ds} = u_{ct} \ln\left(\frac{0.1H}{z_{0m}}\right) / \ln\left(\frac{H}{z_{0m}}\right). \tag{24}$$

Similarly, the equilibrated wind profile would be appropriate to air incident on the downstream wall. The resulting turbulent transport from the wall scales as the vertical average of this wind profile. It follows that there is a minimum bound on the wind speed, u_{dw}, in the isolated roughness and wake interference regimes, which is

$$\min u_{dw} = \left(\frac{u_{ct}}{H - z_{0m}}\right) \int_{z_{0m}}^{H} \ln\left(\frac{0.1H}{z_{0m}}\right) / \ln\left(\frac{H}{z_{0m}}\right) dz. \tag{25}$$

The resistances to transport r_6, r_7 and r_8 (in the isolated roughness region flow regime) are then given as

$$r_6 = \ln\left(\frac{0.1H}{z_{0m}}\right) \ln\left(\frac{0.1H}{z_{0X}}\right) / \kappa^2 u_{ds}, \tag{26}$$

$$r_7 = \frac{\langle \bar{u}(z_r) \rangle - u_{ds}}{u_*^2}, \tag{27}$$

$$r_8 = \ln\left(\frac{0.1H}{z_{0m}}\right) \ln\left(\frac{0.1H}{z_{0X}}\right) / \kappa^2 u_{dw}, \tag{28}$$

where u_* is the friction velocity calculated from the wind profile in the inertial sublayer.

The resistance to transport r_8 in the wake interference flow regime is calculated by taking a weighted average of u_{dw} calculated in the two regions and then linking r_8 to both points B and C in Figure 3.

3.5. Model parameters

The model has five parameters. The surface material roughness lengths, z_{0m} and z_{0X}, are determined by the underlying surface material. Here, for simplicity, $z_{0X} = 0.1 z_{0m}$ is used to represent the relation between the roughness lengths of momentum and heat for the facet surfaces (Garratt, 1992). The two exponents, α_1 and α_2, represent the deceleration of the jet due to the entrainment of slower moving fluid by the jet and frictional effects from the canyon facets. These exponents are found by comparison with the observations, and take the values $\alpha_1 = 0.9$ and $\alpha_2 = 0.15 \max[1, 1.5H/W]$. The second factor in α_2 represents the increase in the deceleration of the jet due to its lack of penetration deep into the canyon cavity at high canyon aspect

ratios as described in Section 2. Here, α_1 is a property of the fluid, and α_2 incorporates a dependence on the surface material roughness. Finally, as explained in Section 2, L_r/H is taken to be 3. The precise value of this ratio is found to have little impact on the model results provided L_r falls in the reasonable range of two to three building heights.

4. Comparison with Observations

The results from the model are now compared with the wind-tunnel measurements from Part I. The buildings are represented as square bars; the variation of the transfer is then measured as the building separation is varied. For this geometry, the planar area index, λ_p, and frontal area index, λ_f, used by Grimmond and Oke (1999b) and others to classify urban areas are given by $\lambda_p = \lambda_f = H/R$. Results are shown here as the transfer velocity for the flux density across a horizontal plane normalised by the wind speed at the top of the boundary layer, U_δ, plotted against the canyon aspect ratio (bottom axis) and the frontal area index (top axis). The comparisons are made by calculating the transfer velocity from the model and comparing directly with the observations. This is done in preference to a comparison of resistances calculated from the observations, as this requires prior knowledge of the model structure. The roughness length for momentum has one value for all four canyon facets, determined by comparison with the observations to be $z_{0m} = 5 \times 10^{-5}$ m.

4.1. Flux from the roof

Figure 6 shows the normalised transfer velocity (w_r/U_δ) for the flux density from the roof facet. The solid line is the model prediction and the symbols are observations from Part I. For H/W greater than about 0.2, both the model and observations indicate that the flux from the roof facet varies little with canyon geometry.

The model shows how the flux varies largely because of the variation of the wind speed in the inertial sublayer with canyon geometry (see Section 3.1 and Figure 5). In the range of the observations, this variation in the wind speed is small resulting in the flat profile. At small H/W, when the building separation becomes large, the wind speed in the inertial sublayer increases, and the flux from the roof correspondingly increases. The transfer from the roof is higher than the transfer from a horizontal surface of the same material calculated using Equations (A3) and (8), which yields $w_{0t}/U_\delta = 2.50 \times 10^{-3}$. At large H/W, as the buildings approach each other and the surface resembles a horizontal surface at building height, the flux from the roof facet asymptotes to that from a horizontal surface of the same material but displaced to roof

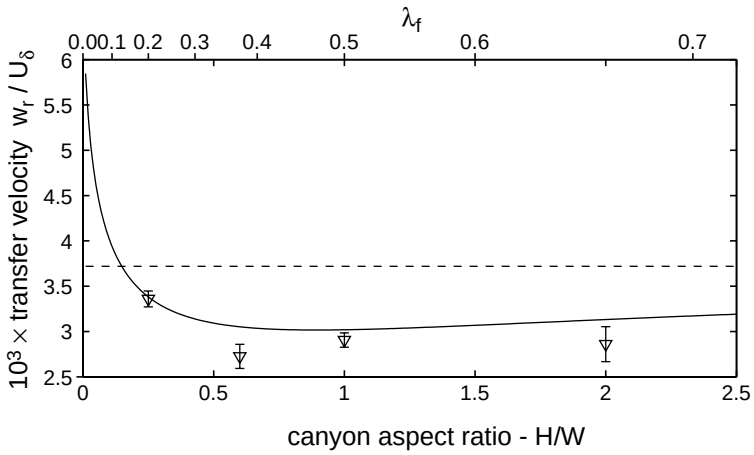

Figure 6. Variation of the transfer velocity for the canyon top flux density for the roof facet normalised by the free stream velocity, w_r/U_δ, with canyon aspect ratio. Solid line, model prediction; triangles, equivalent wind-tunnel measurements taken from Part I. Roughness lengths have the values $z_{0m} = 5 \times 10^{-5}$ m, $z_{0X} = 5 \times 10^{-6}$ m. Dashed line, equivalent prediction from the scaled version of Masson (2000).

level ($w_r/U_\delta = 2.93 \times 10^{-3}$). The asymptote is approached from above and is attained only for very large canyon aspect ratios ($H/W \approx 20$).

4.2. Flux from the street

Figure 7 shows the normalised transfer velocity (w_c/U_δ) across the canyon top, for the flux density from the street facet and its variation with canyon aspect ratio. The solid line is calculated from the model. The symbols are observations from a single street canyon (squares, Barlow and Belcher, 2002) and a series of street canyons (crosses, Part I). The model successfully captures several features in the observations including the dip at $H/W \approx 0.3$, the peak at $H/W \approx 0.6$, and the almost linear decrease as the canyon aspect ratio increases further. The transfer from the street is notably lower than from the roof facet (Figure 6) for all canyon aspect ratios.

The model of the flux from the street facet has the correct limit as the canyon aspect ratio tends to zero, namely that of a horizontal surface of the same material located at $z = 0$, which yields $w_{0t}/U_\delta = 2.50 \times 10^{-3}$. The initial decrease and subsequent general increase in w_c/U_δ as the canyon aspect ratio increases from zero to 0.6 follows the variation in the wind speed in the inertial sublayer (shown in Figure 5). The flow pattern within the street canyon also influences the flux, as explained in Section 3. Firstly, the jet within the recirculation region decelerates as it progresses round the canyon cavity. The deceleration is particularly marked at high canyon aspect ratios,

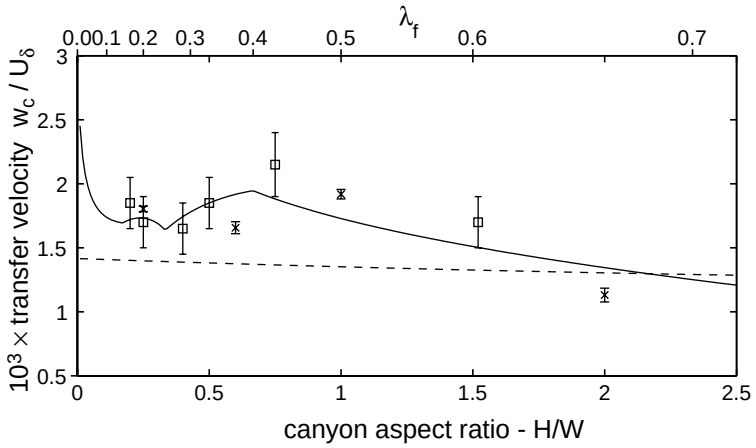

Figure 7. Variation of the transfer velocity for the canyon top flux density from the street facet normalised by the free stream velocity, w_c/U_δ, with canyon aspect ratio calculated from the weighted average of the flux through the recirculation and ventilated regions. Solid line, model prediction; symbols, equivalent wind-tunnel measurements taken from Barlow and Belcher (2002) (squares) and Part I (crosses). Roughness lengths have the values $z_{0m} = 5 \times 10^{-5}$ m, $z_{0X} = 5 \times 10^{-6}$ m. Dashed line, equivalent prediction from the scaled version of Masson (2000).

$H/W > 0.6$, due to the decreased penetration of the jet into the canyon cavity. This explains the reduction in w_c/U_δ when $H/W > 0.6$.

4.3. Flux from the walls

Figure 8 shows the normalised transfer velocities (w_c/U_δ) across a horizontal plane at the canyon top for the flux from the two wall facets. The transfer velocities are expressed in terms of the flux density across the canyon top for ease of comparison with the flux from the street facet. This normalisation introduces a dependence on the relative surface areas of the walls and canyon top, i.e. the ratio H/W, which leads to w_c/U_δ being proportional to H/W.

The flux from the downstream wall is greater than the flux from the upstream wall by approximately a factor of two for all canyon aspect ratios. The difference between the two fluxes, taking the relative surface area into account, is increased as the canyon aspect ratio increases. These two features relate to the variation in turbulent intensity across the street canyon. The downstream wall experiences higher wind speeds and a higher turbulent intensity than the upstream wall for all canyon aspect ratios. The deceleration of the flow around the recirculation region results in reduced flow, and hence reduced turbulent transport from the upstream wall. As for the flux from the street facet, this deceleration is more marked as the canyon aspect ratio

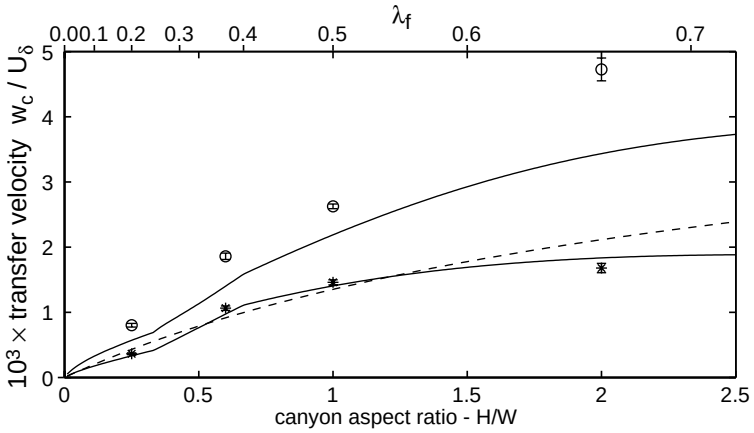

Figure 8. Variation of the transfer velocities for the canyon top flux density from the two wall facets normalised by the free stream velocity, w_c/U_δ, with canyon aspect ratio. Lower solid line, transfer from the upstream wall; upper solid line, transfer from the downstream wall calculated as a weighted average of the flux through the recirculation and ventilated regions; Symbols, equivalent wind-tunnel measurements adapted from Part I for the upstream wall (stars) and downstream wall (circles). Roughness lengths have the values $z_{0m} = 5 \times 10^{-5}$ m, $z_{0X} = 5 \times 10^{-6}$ m. Dashed line, equivalent prediction for both walls from the scaled version of Masson (2000).

increases beyond $H/W \approx 0.6$, which increases the difference in the flux from the two walls.

4.4. Total flux

Figure 9 shows the contribution to the flux through a horizontal plane in the inertial sublayer from each of the canyon facets, normalised by the transfer velocity from a horizontal surface of the same material located at $z = 0$, which has $w_{0t}/U_\delta = 2.50 \times 10^{-3}$. Also shown is the transfer velocity, w_t, associated with the total flux from the canyon surface, calculated using the resistance network and assuming that X takes the same value on all facets. Since the fluxes from the individual canyon facets can interact, w_t is calculated through the resistance network and is not the weighted sum of the individual transfer velocities. Figure 9 therefore shows how much more efficient an urban street canyon is at releasing scalars by turbulent transport than is a flat surface.

The fluxes from each individual facet are smaller than from a horizontal surface for almost all canyon aspect ratios (the transfer from the roof asymptotes ≈ 1.2). The reason is that the canyon geometry reduces the near-surface flow and hence the flux. The total flux is however greater than that from a horizontal surface. This increase is due to the increased surface area,

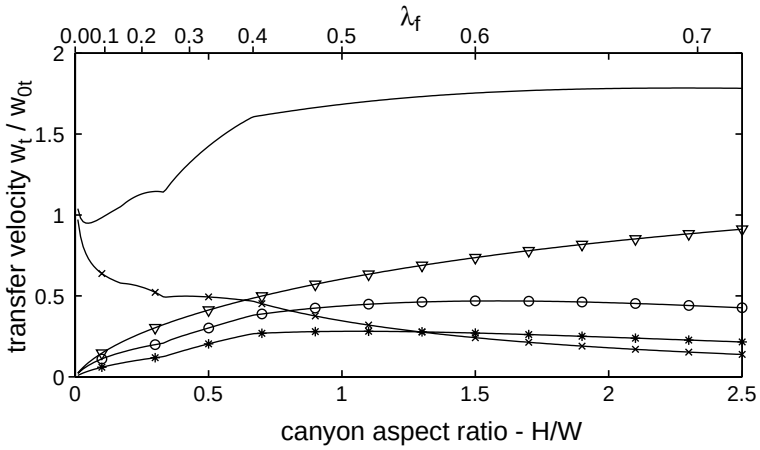

Figure 9. Transfer velocities from each of the facets and the whole canyon surface normalised by the transfer velocity from a flat surface of equivalent surface material properties and total planar area (w_t/w_{0t}). Circles, downstream wall; stars, upstream wall; crosses, street; triangles, roof; solid line, total transport.

indicated by the approximately linear increase in the total flux as the canyon aspect ratio increases from zero to about $H/W = 0.7$. At high canyon aspect ratios, $H/W > 0.7$, the reduction in the near-surface flow is sufficient to reduce the increase in the total flux with total surface area.

Figures 6–8 also show values for the normalised transfer velocities calculated using the model of Masson (2000) with a building height of 10 m (dashed lines). The order of magnitude from the two models agree due to the similarity in the values that common parameters take. The model presented here accounts for the the additional physical processes of the variation of the wind speed in the inertial sublayer as the geometry varies, and the systematic variation in the flow field within the street canyon. Only when these processes are accounted for do the model predictions show the variation with geometry found in the observations.

5. Conclusions

Barlow and Belcher (2002) and Barlow et al. (2004) showed that the vertical flux of a passive scalar from an urban street canyon under transverse flow depends on the geometry of the canyon. The variation with canyon geometry is as much as 50% and differs for each facet of the canyon. This variation is sufficient to warrant inclusion in models of the urban surface energy balance.

The model developed here is based on a partitioning of the canyon air into two distinct regions namely a recirculation region and a ventilated region. The partitioning ensures the correct limit for the transfer velocities as the canyon aspect ratio becomes very small or very large. The individual facets of the canyon flux contribute different amounts implying the need for different representative wind speeds. A single canyon wind speed is unable to reproduce the geometric dependence of all of the facets.

We have shown that there are two principal effects of urban geometry on the flux of a passive scalar from the surface. Firstly, canyon geometry acts to reduce the flow in the inertial sublayer and hence the wind speeds within the vicinity of the street canyon, which then reduces the flux densities from the canyon facets. Secondly, the total surface area of a street canyon is increased compared to a flat surface, which therefore acts to increase the total flux from the surface. These two processes occur regardless of the specific geometry used to represent the urban area.

The model also accounts for streets and buildings made from different materials through the roughness lengths of the underlying surface material. The transfer velocities from the model depend on the ratios z_{0m}/H and z_{0X}/H. Increasing either of these two roughness lengths increases the turbulent transport and increases the magnitude of the peak in the transfer from the street facet. The roughness of one facet can also influence the transfer from the other facets. Increasing the roughness length of the street facet by a factor of ten to simulate the presence of trees, for instance, increases the transfer off the two walls by 0–5%.

The model presented here can be extended to different arrays and geometries of buildings once the pattern of fluid flow is estimated. These processes include three-dimensionality effects, corner vortices and flow separation due to peaked roofs. Such a generalisation remains a task for future work. We hope that our study will stimulate further measurements that can be compared with the present results.

The sensible heat flux is a key term in the surface energy balance. The present work shows how the flux of a scalar, such as sensible heat flux, varies with geometry albeit in neutral conditions only. We suggest that a model for the urban energy balance that is valid over the full range of urban areas will need to account for this variation.

Acknowledgements

It is a pleasure to acknowledge useful conversations with Martin Best and Peter Clark. This work is part of the UWERN Urban Meteorology Programme (web site: www.met.reading.ac.uk/Research/urb_met/). This work is funded by the Natural Environmental Research Council under the

URGENT programme (GST/02/2231) and a NERC CASE studentship with the Met Office (NER/S/A/2000/03555).

Appendix A: The Bulk Aerodynamic Formulation for Surface Fluxes

The time- and spatially-averaged flux density of property X in the inertial sublayer, F_X, is given by

$$F_X = \langle \overline{w'X'} \rangle, \tag{A1}$$

where the primes indicate the instantaneous departure from the mean values, the overbar denotes a time average and the angle brackets a spatial average. If the flux of X is effected entirely by turbulence, dimensional analysis shows that the flux is proportional to the difference of the mean values X takes at the surface and at some height above that surface and to a transport velocity. This approach of relating the flux of X to the mean values of X is the bulk aerodynamic formulation (Garratt, 1992). Denoting the area-averaged value of X at the surface by $\langle \overline{X}_s \rangle$ and at any height, z, in the inertial sublayer, $\langle \overline{X} \rangle$, the flux density of X at the surface, F_X, is given by

$$F_X = w_X\big(\langle \overline{X}_s \rangle - \langle \overline{X} \rangle\big) = \frac{\langle \overline{X}_s \rangle - \langle \overline{X} \rangle}{r_X}, \tag{A2}$$

where w_X is the transfer velocity for property X and its reciprocal, r_X, is the resistance to transport.

For a neutrally stratified rough-wall boundary layer with zero displacement height that is in equilibrium with the underlying surface, the mean wind profile, $\langle \bar{u}(z) \rangle$, and profile of X, $\langle \overline{X}(z) \rangle$, are,

$$\langle \bar{u}(z) \rangle = \frac{u_*}{\kappa} \ln\left(\frac{z}{z_{0m}}\right), \tag{A3}$$

$$\langle \overline{X}(z) \rangle - \langle \overline{X}_s \rangle = \frac{X_*}{\kappa} \ln\left(\frac{z}{z_{0X}}\right), \tag{A4}$$

where $u_* = (\tau/\rho)^{1/2}$ is the friction velocity, $X_* = -F_X/u_*$ is a scaling for X', κ is the von Kármán constant and z_{0m} and z_{0X} are the roughness lengths for momentum and property X respectively. The resistance to the transport of X therefore takes the form

$$r_X(z) = \ln\left(\frac{z}{z_{0m}}\right) \ln\left(\frac{z}{z_{0X}}\right) \Big/ \kappa^2 \langle \bar{u}(z) \rangle. \tag{A5}$$

Within the inertial sublayer of the atmospheric boundary layer the area-averaged flux density is uniform with height and therefore takes the same

value as at the surface. Using Equation (A5) at two heights, $z_1 < z_2$, within the inertial sublayer, the flux density of X at the surface can be related to the mean profile of X by

$$F_X = w_{X\Delta}\big(\langle\overline{X}(z_1)\rangle - \langle\overline{X}(z_2)\rangle\big) = \frac{\langle\overline{X}(z_1)\rangle - \langle\overline{X}(z_2)\rangle}{r_X(z_r) - r_X(z_1)}. \tag{A6}$$

Using Equations (A3)–(A6) the resistance to transport between the two atmospheric levels, $r_{X\Delta} = r_X(z_r) - r_X(z_1)$, can be expressed as

$$r_{X\Delta} = \frac{\Delta\langle\overline{X}\rangle}{u_* X_*}. \tag{A7}$$

In a boundary layer where the mean vertical profiles of all properties can be described by Equation (A4), as determined by the relevant roughness lengths, $r_{X\Delta}$ takes the same value regardless of the property considered.

A boundary layer undergoing an adjustment to new surface properties forms an internal boundary layer; the profile of X in such a region can be considered to form three sublayers. The inner-most layer is in full equilibrium with the underlying surface, the outer-most layer remains unaffected by the change in surface properties, with the middle layer blending the two profiles together. The depth of the internal boundary layer relates to the distance downstream from the change in surface properties; this dependence is taken to be linear. The turbulent transport from the surface to a height in the outer layer depends on both the resistance to transport from the surface, r_1, and the resistance to transport across the internal boundary layer, r_{12}, as shown schematically in Figure 10. If the wind speed at height z_1 is known, r_1 is given by Equation (A5). The resistance to transport r_{12} is given by Equation (A7) where now u_* and X_* are the local scaling terms. These local scaling terms are approximated by those of the outer layer, as transport is dominated by the larger eddies that will have this characteristic scaling.

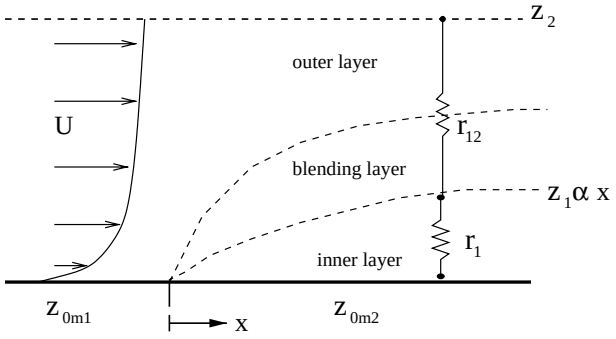

Figure 10. Schematic of the resistance network across a developing internal boundary layer.

In an adjusting boundary layer it is not immediately obvious that Equation (35) takes the same value for all properties X. In fact, assuming Equation (35) holds for the transport of momentum, the resistance to transport of property X depends on the ratio $r_{X\Delta}/r_{u_\Delta}$: when considering heat this ratio is the turbulent Prandtl number. For small-scale turbulence and turbulence in a free shear layer the turbulent Prandtl number is approximately 1 (Tennekes and Lumley, 1997, p. 51). It follows that the resistance to transport of heat across a free shear layer is given by $r_{T\Delta} = \Delta u/u_*^2$, where the friction velocity is that of the outer layer.

References

Arnfield, A. J.: 2003, 'Two Decades of Urban Climate Research: A Review of Turbulence, Exchanges of Energy and Water, and the Urban Heat Island', *Int. J. Climatol.* **23**, 1–26.

Arnfield, A. J. and Grimmond, C. S. B.: 1998, 'An Urban Canyon Energy Budget Model and its Application to Urban Storage Heat Flux Modelling', *Energ. Buildings* **27**, 61–68.

Baik, J.-J., Park, R. -S., Chun, H. -Y., and Kim, J. -J.: 2000, 'A Laboratory Model of Urban Street–Canyon Flows', *J. Appl. Meteorol.* **39**, 1592–1600.

Barlow, J. F. and Belcher, S. E.: 2002, 'A Windtunnel Model for Quantifying Fluxes in the Urban Boundary Layer', *Boundary-Layer Meteorol.* **104**, 131–150.

Barlow, J. F., Harman, I. N., and Belcher, S. E.: 2004, 'Scalar Fluxes from Urban Street Canyons. Part I: Laboratory Simulation', *Boundary-Layer Meteorol.* **113**, 369–385.

Best, M.: 1998, 'A Model to Predict Surface Temperatures', *Boundary-Layer Meteorol.* **88**, 279–306.

Best, M.: 1999, 'Can We Represent Urban Areas in Operational Numerical Weather Prediction Models?', in *Proceedings of the Third Urban Environment Symposium*, pp. 70–71.

Brown, M. J., Lawson, R. E., Decroix, D. S., and Lee, R. L.: 2000, 'Mean Flow and Turbulence Measurements around a 2-D Array of Buildings in a Wind Tunnnel', in *11th Joint AMS/AWMA Conference on the Applications of Air Pollution*, Long Beach, CA.

Castro, I. P. and Robins, A. G.: 1977, 'The Flow around a Surface-Mounted Cube in Uniform and Turbulent Streams', *J. Fluid Mech.* **79**, 307–335.

Caton, F., Britter, R. E., and Dalziel, S.: 2003, 'Dispersion Mechanisms in a Street Canyon', *Atmos. Environ.* **37**, 693–702.

Cheng, H. and Castro, I. P.: 2002, 'Near Wall Flow over an Urban-like Roughness', *Boundary-Layer Meteorol.* **104**, 229–259.

Garratt, J. R.: 1992, *The Atmospheric Boundary Layer* (Chapter 8, pp. 224–257), Cambridge University Press, U.K., 316 pp.

Grimmond, C. S. B. and Oke, T. R.: 1999a, 'Aerodynamic Properties of Urban Areas Derived from Analysis of Surface Form', *J. Appl. Meteorol.* **38**, 1262–1292.

Grimmond, C. S. B. and Oke, T. R.: 1999b, 'Heat Storage in Urban Areas: Local-Scale Observations and Evaluation of a Simple Model', *J. Appl. Meteorol.* **38**, 922–940.

Grimmond, C. S. B. and Oke, T. R.: 2002, 'Turbulent Heat Fluxes in Urban Areas: Observations and a Local-Scale Urban Meteorological Parameterization Scheme (LUMPS)', *J. Appl. Meteorol.* **41**, 792–810.

Grimmond, C. S. B., Cleugh, H. A., and Oke, T. R.: 1991, 'An Objective Urban Heat-Storage Model and its Comparison with Other Schemes', *Atmos. Environ.* **25B**, 311–326.

Hertel, O. and Berkowicz, R.: 1989, *Modelling Pollution from Traffic in a Street Canyon. Evaluation of Data and Model Development*, Technical Report DMU LUFT-A129, National Environmental Research Institute, Denmark.

Hogg, A. J., Huppert, H. E., and Dade, W. B.: 1997, 'Erosion by Planar Turbulent Wall Jets', *J. Fluid Mech.* **338**, 317–340.

Johnson, G. T. and Hunter, L. J.: 1995, 'A Numerical Study of the Dispersion of Passive Scalars in City Canyons', *Boundary-Layer Meteorol.* **75**, 235–262.

Johnson, G. T., Oke, T. R., Lyons, T. J., Steyn, D. G., Watson, I. D., and Voogt, J. A.: 1991, 'Simulation of Surface Urban Heat Islands under 'Ideal' Conditions at Night. Part 1: Theory and Tests against Field Data', *Boundary-Layer Meteorol.* **56**, 275–294.

Kusaka, H., Kondo, H., Kikegawa, Y., and Kimura, F.: 2001, 'A Simple Single-Layer Urban Canopy Model for Atmospheric Models: Comparison with Multi-Layer and Slab Models', *Boundary-Layer Meteorol.* **101**, 329–358.

Louka, P., Belcher, S. E., and Harrison, R. G.: 2000, 'Coupling between Air Flow in Streets and in the Well-Developed Boundary Layer Aloft'. *Atmos. Environ.* **34**, 2613–2621.

Macdonald, R. W., Griffiths, R. F., and Hall, D. J.: 1998, 'An Improved Method for the Estimation of Surface Roughness of Obstacle Arrays', *Atmos. Environ.* **32**, 1857–1864.

Martilli, A., Clappier, A., and Rotach, M. W.: 2002, 'An Urban Surface Exchange Parameterisation for Mesoscale Models', *Boundary-Layer Meteorol.* **104**, 261–304.

Masson, V.: 2000, 'A Physically-Based Scheme for the Urban Energy Budget in Atmospheric Models', *Boundary-Layer Meteorol.* **94**, 357–397.

Masson, V., Grimmond, C. S. B., and Oke, T. R.: 2002, 'Evaluation of the Town Energy Balance (TEB) Scheme with Direct Measurements from Dry Districts in two cities', *J. Appl. Meteorol.* **41**, 1011–1026.

Mills, G. M.: 1993, 'Simulation of the Energy Budget of an Urban Canyon – I. Model Structure and Sensitivity Test', *Atmos. Environ.* **27B**, 157–170.

Nakamura, Y. and Oke, T. R.: 1988, 'Wind, Temperature and Stability Conditions in an East–West Oriented Urban Canyon', *Atmos. Environ.* **22**, 2691–2700.

Narita, K.: 2003, 'Wind Tunnel Experiment on Convective Transfer Coefficient in Urban Street Canyon', in *Proceedings of the Fifth International Conference on Urban Climate*, Łódź, *Poland.*

Nunez, M. and Oke, T. R.: 1977, 'The Energy Balance of an Urban Canyon', *J. Appl. Meteorol.* **16**, 11–19.

Okamoto, S., Nakaso, K., and Kawai, I.: 1993, 'Effect of Rows of Two-Dimensional Square Ribs of Flow Property along Plane Wall', *JSME Int. J. Series B. – Fluid Therm. Engin.* **36**, 121–129.

Oke, T. R.: 1987, *Boundary Layer Climates* (Chapter 8, pp. 262–303), Routledge, 2nd edn., Methuen, New York, 435 pp.

Oke, T. R.: 1988, 'Street Design and Urban Canopy Layer Climate', *Energ. Buildings* **11**, 103–113.

Raupach, M. R., Antonia, R. A., and Rajagopalan, S.: 1991, 'Rough-Wall Turbulent Boundary Layers', *Appl. Mech. Rev.* **44**, 1–25.

Sakakibara, Y.: 1996, 'A Numerical Study of the Effect of Urban Geometry upon the Surface Energy Budget', *Atmos. Environ.* **30**, 487–496.

Sini, J.-F., Anquetin, S., and Mestayer, P. G.: 1996, 'Pollutant Dispersion and Thermal Effects in Urban Street Canyons', *Atmos. Environ.* **30**, 2659–2677.

Tennekes, H. and Lumley, J. L.: 1997, *A First Course in Turbulence* (Chapter 2, pp. 27–58), The MIT Press, Cambridge, MA, 300 pp.

Townsend, A. A.: 1976, *The Structure of Turbulent Shear Flow* (Chapter 7. Boundary Layers and Wall Jets, pp. 259–333), 2nd edn., Cambridge University Press, U.K., 429 pp.